Discovery of an Optimal Porous Crystalline Material for the Capture of Chemical Warfare Agents

Ismael Matito-Martos,[#,a,b] Peyman Z. Moghadam,[#,*,b] Valentina Colombo,[c] Jorge A. R. Navarro,[d]

Sofia Calero,[*,a] and David Fairen-Jimenez[*,b]

[a]Department of Physical, Chemical and Natural Systems, University Pablo de Olavide, Sevilla 41013, Spain

[b]Adsorption & Advanced Materials Laboratory (AAML), Department of Chemical Engineering and Biotechnology, University of Cambridge, Philippa Fawcett Drive, Cambridge CB3 0AS, United Kingdom

[c]Department of Chemistry, University of Milan, Milan 20133, Italy

[d]Department of Inorganic Chemistry, University of Granada, Granada 18071, Spain

Abstract

Chemical warfare agents (CWAs) are regarded as a critical challenge. Here, we use a high-throughput computational screening strategy backed up by experimental validation to identify and synthesize a promising porous material for CWA adsorption and removal under humid conditions. Starting with a database of 2,932 existing metal-organic frameworks (MOF) structures, we selected those possessing cavities big enough to adsorb well-known CWAs such as sarin, soman, and mustard gas as well as their non-toxic simulants. We used Widom method to reduce significantly the simulation time of water adsorption, allowing us to shortlist 156 hydrophobic MOFs were water will not compete with the CWAs to get adsorbed. We then moved to grand canonical Monte Carlo (GCMC) simulations to assess the removal capacity of CWAs. We selected the best candidates in terms of performance but also in terms of chemical stability, and moved to synthesis and experimental breakthrough adsorption to probe the predicted excellent performance. This computational-experimental work represents a fast and efficient approach to screen porous materials in applications that involve moisture presence.

KEYWORDS: Metal-organic frameworks, Water adsorption, GCMC, Chemical warfare agents, Toxic industrial chemicals

1. Introduction

Chemical warfare agents (CWAs) are highly toxic compounds designed to cause harm, death, temporary incapacitation or sensory irritation through their chemical actions. CWAs were used during World War I,[1] and since then the threat has continuously evolved with the development of increasingly more toxic chemicals. Even though their use is strictly prohibited according to the Chemical Weapons Convention of 1993, protection against deliberate attacks using CWAs is still regarded as a critical challenge.[2] In particular, CWAs such as sarin and soman – two well-known nerve agents – and mustard gas – a vesicant compound – have received great attention due to its relative easy accessibility.[3] Nowadays, efforts for the elimination of chemical weapons are continuously increasing, something that has been recognized with e.g. the prestigious Nobel Peace Prize to the Organization for the Prohibition of Chemical Weapons

1

(OPCW) in 2013. Nevertheless, population exposure has occurred recently with nerve gas attacks in Syria in August 2013, in April 2017, and more recently in April 2018.[4]

In order to reduce the risk of exposure, the development of suitable capture methods for a wide range of chemical threats is highly necessary. Historically, activated carbons (ACs) have been used for CWAs and small toxic industrial chemicals (TICs) capture. One of the most important drawbacks of ACs, however, is their low adsorption capacity.[2,5-7] In addition, to afford broad spectrum of utility, ACs are generally impregnated with a variety of acidic and basic compounds that inherently react between them over time, reducing their efficacy.[2] An alternative that has arisen in the last years is the use of metal-organic frameworks (MOFs) for the capture of CWAs, a possibility that has been extensively explored both experimentally and using molecular simulation.[8-14] MOFs are porous crystalline materials built from metal or metal-based clusters linked by organic ligands to form a three-dimensional structure.[15-18] MOFs exhibit a considerable degree of tunability, not only due to the wide diversity of possible inorganic and organic components that can be included, but also via post-synthetic modification of their structures.[19] Indeed, in a recent collaboration with the Cambridge Cyrstallographic Database Centre we have identified ca. 80,000 MOFs already synthesized – a number that will continue growing every year.[20] The high tunability of MOFs allows an oriented control and design of structural features such as pore size and geometry, surface area and surface chemistry, which results in unbeaten adsorptive and catalytic properties,[21,22] including the capture and/or decomposition of harmful volatile chemicals.[8-13]

In spite of their potential, a main limitation for finding optimal MOFs for CWA and TIC capture relies in obvious health and safety complications, and therefore experimental studies are rather scarce.[2] Often, testing CWAs is very expensive and not universally available, and therefore most of the studies are based on a surrogate chemical, commonly called simulant or analogue, that possesses most of the key features of the real agent.[5] Bobbitt *et al.* recently reviewed the experimental and computational studies about the use of MOFs for detoxification applications of CWAs and TICs.[14] For example, Zou *et al.* reported the synthesis of a MOF with an extremely high capacity for the capture of the nerve agent simulant methylphosphonic acid (MPA).[23] More recently, Montoro *et al.* compared the suitability of a hydrophobic Zn pyrazolate-based MOF against the hydrophilic HKUST-1 to capture sarin and mustard simulants (diisopropylfluorophosphate, DIFP, and diethylsulfide, DES, respectively). This work showed that, although the coordinatively unsaturated metal sites present in HKUST-1 result in an outstanding performance in dry conditions, their efficiency dropped in the presence of ambient moisture.[3] Following a similar approach, Padial *et al.* reported the suitability of a series of Ni pyrazolate-based MOFs for the capture of DES under the presence of moisture.[24] Plonka *et al.* reported Zr-MOFs as being effective adsorbents of CWAs from air,[7] whereas Mondloch *et al.*[25] and Moon *et al.*[26] used Zr-based NU-1000 for the catalytic destruction of soman. Importantly, in all these studies, competitive adsorption of water from atmosphere emerges as an unavoidable challenge that can significantly affect CWAs capture performance of MOFs and other porous materials. A potential solution to this challenge is the use of hydrophobic materials that selectively adsorb CWAs and TICs in competition with water.[27] By using hydrophobic MOFs, the pores can potentially remain empty, avoiding water adsorption, while maintaining their adsorption capability for CWAs.

Given the large number of existing MOFs,[20] the use of molecular simulations has demonstrated to be an outstanding tool for high-throughput screening (HTS) of them.[28] In particular for CWAs and TICs, computational work also avoids the experimental complications associated with toxic compounds. Recently, Ghosh *et al.* used grand canonical Monte Carlo (GCMC) simulations to predict water adsorption in a series of MOFs, using the pressure at which water condenses in the pores as indicator of their hydrophobicity.[11] However, screening large number of materials using this criterion is computationally too expensive and very time consuming due to long water equilibration times in GCMC

simulations – typically in the order of 1 month per pressure point in an adsorption isotherm.[12] We recently proposed an alternative method to use the more easily calculated water Henry´s constants (K_H) as and efficient tool for calculating the hydrophobicity for porous materials and for HTS of a large number of structures.[12] K_H describes the zero loading region of the isotherm (i.e. the Henry region), giving information about adsorbate-adsorbent interactions. K_H is usually obtained from the slope of the adsorption isotherm at low loadings, but can be also quickly computed using the Widom insertion method.[29] This method provides reliable K_H values and, critically, is orders of magnitude faster (e.g. minutes vs. months) than those calculated from GCMC adsorption isotherms.

In this work, we explored the use of HTS to study the capture of three CWAs: sarin, soman, and mustard gas (Figure 1) in the presence of moisture. The tern mustard gas refers to a wide variety of chemical compounds and mixtures. However, it usually points to HD, composed by bis(2-chloroethyl) sulfide approximately 96% pure. For this reason, we will refer to this molecule when we talk about mustard gas in the rest of the work. We have also extended the study to their simulants, commonly used in experiments: diisopropylfluorophosphate (DIFP), dimethyl methylphosphonate (DMMP), and diethylsulfide (DES). We used Widom insertion to screen 1,647 MOF structures to identify the most suitable materials for CWA capture. We also included water adsorption in order to discard those materials in which the presence of water would fill their porosity and reduce the CWAs capture under humid conditions. We further explored the storage capacity of 156 top-performing MOFs using GCMC simulations to highlight the best candidates for this application, and compared our results with experimental findings.
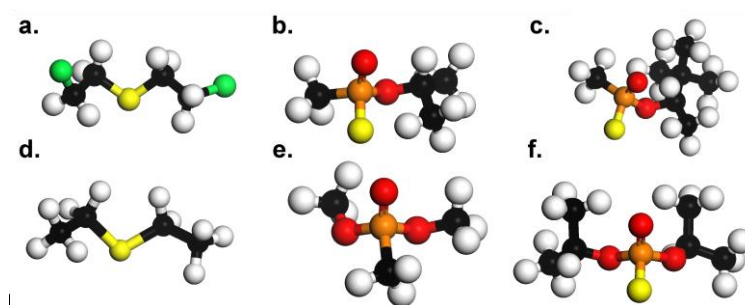

Figure 1. Atomic representation of the CWA molecules: **a.** mustard gas, **b.** sarin, and **c.** soman; and their respective simulants **d.** diethylsulfide (DES), **e.** dimethyl methylphosphonate (DMMP), and **f.** diisopropylfluorophosphate (DIFP). Carbon, oxygen, chlorine, fluorine, phosphorus and hydrogen atoms are depicted in black, red, green, yellow, orange and white, respectively.

2. Results and Discussion

The CSD MOF subset contains over 80,000 structures as of November 2017.[20] However, since high quality partial charges are critical to get meaningful adsorption isotherms for polar compounds, we focused on the materials provided by the DDEC database containing 2,932 porous structures where the framework charges were accurately calculated.[30] Figure S1 shows a summary of the geometric characterization of each MOF structure: largest cavity diameter (LCD), pore volume (PV), and helium void fraction (HVF). Out of these 2,932 structures, some of them exhibit too narrow pores to be useful in our study, and therefore we excluded 1,275 structures with pore limiting diameters (PLDs) lower than 3.72 Å.[31] Figure S1 shows the gravimetric surface area (GSA) histograms for the 1,647 remaining MOFs.

To estimate efficiently the strength of the MOF-CWA interactions at low coverage we used Widom insertion to obtain, for all 1,647 MOFs, the K_H and isosteric heat of adsorption (Q_{st}) for the CWAs, their

simulants, and water at room temperature. By using Widom insertion we were able to reduce significantly the computational time required, compared to standard GCMC simulations. Figure 2 delimits the relationship between K_H, Q_{st} and the LCD of the studied MOFs for the three CWA and simulant molecules. For mustard and its simulant (Figure 2a), K_H span from ca. 10^{-4} to ca. 10^{12} mol·kg^{-1}·Pa^{-1}. Both molecules show a similar trend, although the interaction is slightly stronger for the mustard gas compared to DES; this can be attributed to the fact that mustard gas is a bulkier molecule. In general, MOFs with LCDs around 5 Å show the highest K_H values, while the interactions decrease for materials with LCD values larger than 8 Å (e.g. $K_H < 10^4$ mol·kg^{-1}·Pa^{-1}). Figure 2d shows a comparison between the Q_{st} for mustard gas and DES, confirming the good correlation between their adsorption behaviors and the relationship with the LCD. Q_{st} ranges from 30 to 130 kJ·mol^{-1}, with values lower than 80 kJ mol^{-1} for MOFs with LCDs larger than 8 Å, and the highest Q_{st} values are found in MOFs with cavities of around 5 Å. Figures 2b-d and 2c-f show the results for sarin and DMMP, and soman and DIFP, respectively. We found larger K_H values for these molecules compared to mustard gas – going to extreme values as high as 10^{30} mol·kg^{-1}·Pa^{-1}. In terms of Q_{st}, the highest values are obtained for LCD around 5-6 Å, where Q_{st} ranges between 50 and 200 kJ·mol^{-1} for soman and DIFP, and ca. 250 kJ·mol^{-1} for sarin and DMP. Differences in shape and size of these two pairs of molecules are more evident, resulting in a slightly poorer correlation between the CWAs and their simulants compared to mustard gas-DES pair. The biggest differences are observed in Figure 2f. In this figure the Q_{st} of the simulant differs significantly from the CWA for MOFs with LCDs around 5-6 Å. For this couple, related differences in molecular shape and size are the highest and that makes possible that DIFP is able to fit closely in some structures with narrow LCDs in which soman is not able to fit well. Figure S2 shows the Q_{st} for the CWAs on each MOF as a function of GSA and LCD. The highest Q_{st} values are found in structures with quite low surface areas (< 1000 m^2·g^{-1}), while the strength of the interaction remains high in structures with surface areas up to 2000 m^2·g^{-1}. Mustard gas, soman, and sarin reach Q_{st} values up to 100, 160 and 200 kJ·mol^{-1} in these MOFs.
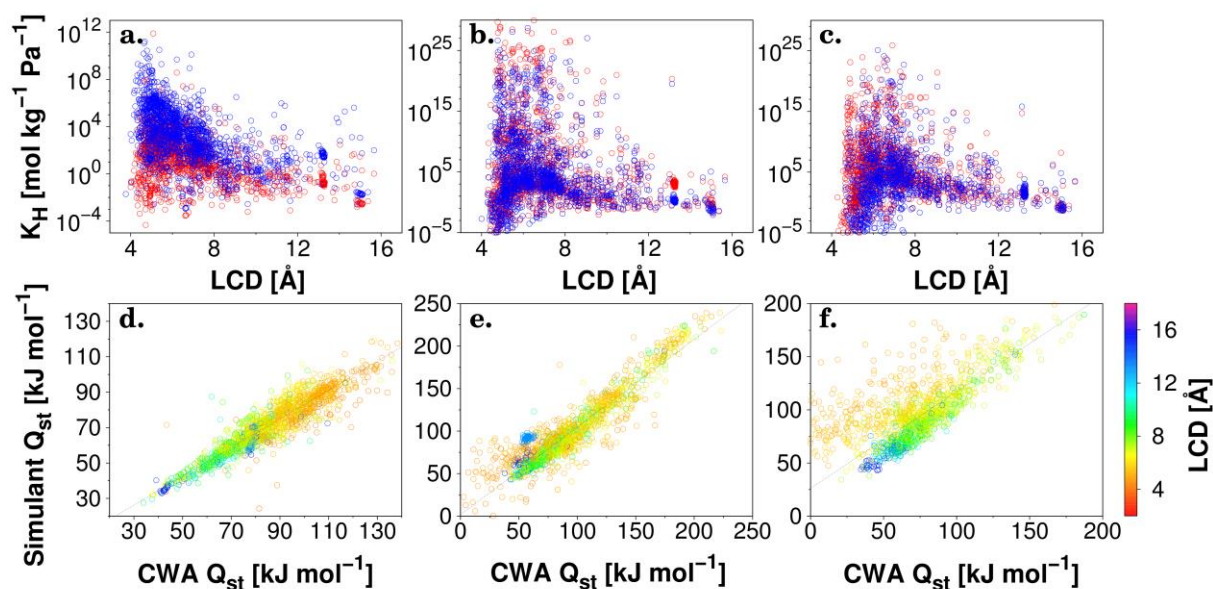

Figure 2. Henry´s constants (K_H) as a function of the largest cavity diameter (LCD) of 1,647 MOFs for: **a**. mustard gas and DES, **b.** sarin and DMMP, and **c.** soman and DIFP. Blue and red data points represent the CWA and the simulant, respectively. **d., e., f.** Comparison of the heat of adsorption (Q_{st}) for each CWA and simulant. Color code represents the LCD of MOF structures. All simulations were performed at 298 K.

This preliminary HTS is useful to map the interactions between MOFs and CWAs/simulants and to understand the goodness of the simulants to substitute CWAs in experiments and simulations. However, as stated above, the suitability of MOFs to achieve an efficient removal of CWAs needs to be evaluated under humid conditions in the presence of water. To address this problem, we studied the water affinity of the 1,647 MOFs through the estimation of Q_{st} and K_H, using Widom insertion method[29] – avoiding highly time-consuming GCMC simulations. Figure S3 shows the K_H and Q_{st} for water as a function of LCD. We included two benchmarks for comparison: the well-known hydrophobic MOF ZIF-8,[12] and the hydrophilic MOF HKUST-1[32]. Figure 3 highlights the MOFs exhibiting K_H below the upper limit given by HKUST-1, assuming that MOFs with higher K_H will be saturated with water at 80% relative humidity. From all the 1,647 MOFs screened, we identified 156 hydrophobic structures (ca. 9.5% of all studied MOFs) with K_H and Q_{st} values lower than that of ZIF-8 (i.e. $5 \cdot 10^{-6}$ mol·kg^{-1}·Pa^{-1} and 30 kJ·mol^{-1}, respectively).[12,33] 937 MOFs (57.0%) were more hydrophilic than HKUST-1 (i.e. $K_H > 5 \cdot 10^{-2}$ mol·kg^{-1}·Pa^{-1} and $Q_{st} > 40$ kJ·mol^{-1}), whereas 554 MOFs (33.6%) exhibit and intermediate hydrophobic character between ZIF-8 and HKUST-1.
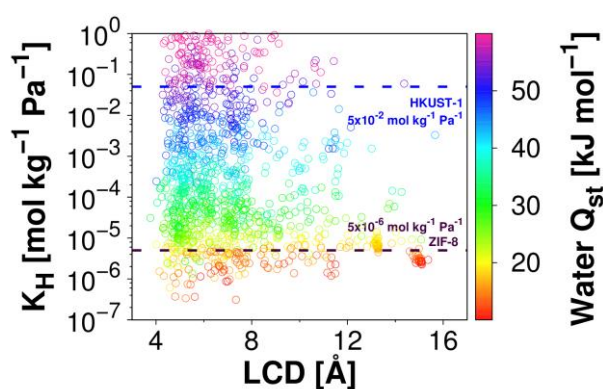

Figure 3. Henry´s constants (K_H) for water as a function of the largest cavity diameter (LCD) in MOF structures with K_H lower than 1 mol·kg^{-1}·Pa^{-1} at 298 K. Purple and blue dashed lines depict water K_H in ZIF-8 and HKUST-1, respectively, as benchmarks for hydrophobicity and hydrophilicity in MOFs. Color code represents isosteric heat of adsorption (Q_{st}) for water.

Figure 4 shows the selectivity for mustard gas, sarin, and soman over water as a function of the gravimetric surface area for the 1,647 MOF structures studied here. The evaluation of water Q_{st} (top) and LCD (down) has been also included as color graduation. For direct comparison, the same representation has been included in Figure S4 for each respective CWA simulant. In general, most of the non-CWA selective structures exhibit very low surface area (< 1,000 m2·g-1), which may suggest that either the pores are too small for CWA molecules, or that the porosity and interaction are optimal for water adsorption. MOF selectivities go up to 106 independently of the surface area. Depending on the CWA, the selectivity has a stronger influence by water affinity (mustard gas and DES, Figs. 4a and 4d, and Figs. S4a and 4d, respectively), LCD (soman and DIFP, Figs. 4b and 4e, and Figs. S4b and 4e, respectively) or both (sarin and DMMP, Figs. 4c and 4f, and Figs. S4c and 4f, respectively). To explain it better, we also plotted in Figure S5 the impact of CWA affinity on selectivity. In the case of mustard and DES, the hydrophobicity of the MOFs has a very strong influence in the selectivity, as can be observed comparing the figures. While MOFs with similar CWA affinity show different total selectivity (Fig S5), the points seen to be very ordered as s function of water affinity (Figs 4a and S4a). This is probably related to the hydrophobic nature of both molecules, making that in general they do not

compete for the same structures with water. However, the more hydrophilic nature of the nerve agent molecules and their simulants make that in some case they compete very strongly with water for some MOFs structures. For this reason, while in the case of mustard and DES the CWA affinity does not seem to show any correlation with the selectivity, the CWA affinity is strongly correlated with the selectivity for nerve agents like molecules. This can be particularly observed for sarin and its simulant, for which the structures with the highest CWA affinity (pink points with very high selectivity in Fig S5b and e) also show moderate water affinity (Figs 4a and S4a). The existence of some structures with high CWA affinity in combination with moderate water affinity confirms the importance of taking into account this latter parameter in combination with the chemical affinity for the selection of materials to avoid water pore filling at atmospheric conditions. Discarding these MOFs with moderate water affinity, the MOFs with the best performance in terms of high selectivity and high surface area are in good agreement with the 156 hydrophobic MOFs previously identified according to water KH and Qst criteria.
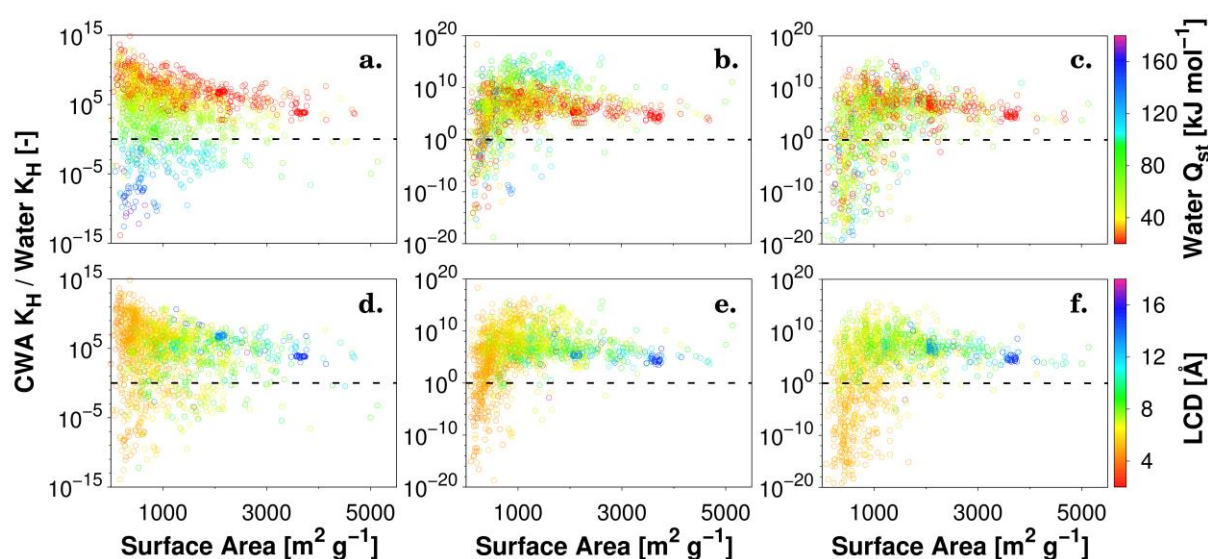

Figure 4. Selectivity of **a., d.** mustard gas, **b., e.** sarin, and **c., f.** soman over water based on the K_H ratio as a function of the surface area in 1,647 MOF structures. The color code shows the isosteric heat of adsorption (Q_{st}) for water (**a-c**) and largest cavity diameter (**d-f**) for each MOF structure.

Although the high surface areas of top-performing MOFs in terms of selectivity indicates that we are far away from Henry´s regime during CWA adsorption, using this approach (i.e. evaluating selectivity using the ratio of K_H) is valid for hydrophobic materials, since water will not be adsorbed. To probe that, we ran computationally demanding GCMC simulation of water adsorption at 80% relative humidity (i.e. at 3,280 Pa based on the vapor pressure predicted for the TIP4P water model) on the selected 156 hydrophobic MOFs identified from the water Widom screening (Figure S6). GCMC simulation confirms the extremely low water adsorption in the selected hydrophobic MOFs, with less than 0.1 mol·kg^{-1} in almost all structures; it also confirms the goodness of the Widom approach and its applicability on fast preselection screening while ensuring minimized competitive water adsorption even at high humidity (RH=80%). We continued with the GCMC simulation of mustard gas (at 13.8 Pa)[34–36] and nerve agents (at 0.6 Pa),[37,38] according to reported median lethal concentration-time product (LCt$_{50}$) at respiratory level for these molecules. Figure 5 shows the loading capacity of mustard gas, sarin, and soman as a function of the CWA/water Widom selectivity and surface area. Additionally, Figure S7 also

6

The 156 selected hydrophobic MOFs show very high selectivities, particularly for structures with surface areas below 1,000 $m^2 \cdot g^{-1}$ and high Q_{st}. As expected, adsorption loadings are strongly related to surface area, where the highest loadings, up to 8 $mol \cdot kg^{-1}$, are found in MOFs with surface areas larger than 2,000 $m^2 \cdot g^{-1}$ as illustrated by the dark blue and purple data points. Loading capacities are also highly dependent on LCD, which in turns directly influence CWA affinity (Figure S7). Larger LCDs (generally >12 Å) and surface areas allow maximizing loading capacities, while smaller pores limit their performance in spite of the increase in CWA Q_{st} values and K_H selectivities.
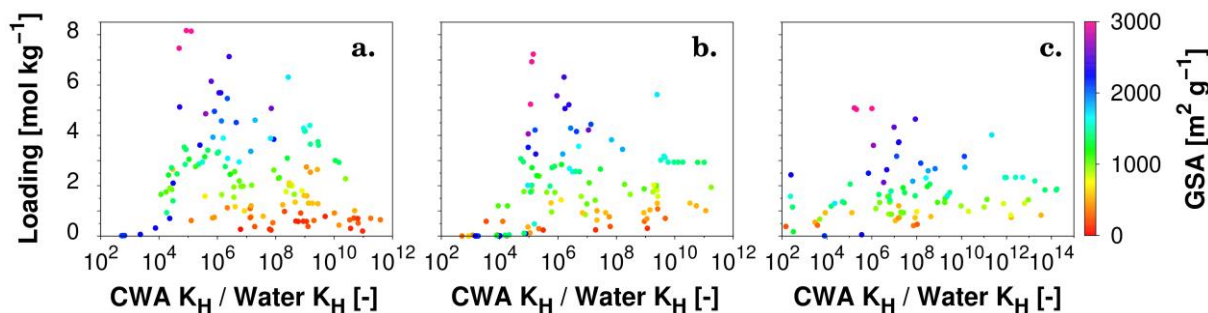

Figure 5. GCMC calculated loadings for **a.** mustard, **b.** sarin, and **c.** soman adsorption at 13.8 Pa (mustard) and 0.6 Pa (sarin and soman), as a function of selectivity over water based on Henry´s constants (K_H/K_H). Each point represents one of the 156 hydrophobic MOFs studied at 298 K. The color code shows the surface area of each MOF.

To identify promising MOFs capable of capturing a wide range of CWAs, we compared the loading capacities for mustard gas and the nerve agents, represented in Figure 6a. Interestingly, we found an excellent correlation for the loadings of the different CWAs. This minimizes the experimental synthesis and characterization of MOFs, since identifying an optimal structure that is good for capturing one CWA means that it will be also optimal for the other two. At this point we shortlisted the top eight structures with CWA capacities higher than 4 $mol \cdot kg^{-1}$. We then took a number of considerations into account to propose candidates for experimental testing. In general, a combination of high surface area, high pore volume and ease of synthesis are important requirements for practical applications. Besides, water stability and surface hydrophobicity are crucial for capture and removal processes that involve moisture. From the eight shortlisted MOFs, we found four structures (CSD codes: BIBXUH,[24] SOHGUS,[39] Co26NDP[‡] and UTEWOG[40]) with metal-pyrazolate coordinative bonds, that are known to impart high thermal and, in some cases, chemical stability in MOFs.[41] However, from a close look on their crystal structures, we found out that SOHGUS is a DMF-solvated form of COJHIT, Long's CoBDP (where BDP^{2-} = 1,4-benzenedipyrazolate) flexible MOF[39] – a well-known pyrazolate-flexible MOF that has been tested for methane storage.[42] However, we decided to reject this MOF since it is unstable, and decomposes in air after few minutes. Additionally, we discarded three structures (CSD codes: HIGRIA, BICDAU, and IVETOT) that although present optimal performance, they are reported to collapse upon activation.[43] IRMOF-6 (CSD code: EDUTIG) was also discarded because of its low water stability.[17] All in all, we ended with three top MOF candidates (CSD codes: BIBXUH, Co26NDP[‡], and UTEWOG); Figures 6b and S8-S9 show the representation of UTEWOG, and BIBXUH and Co26NDP[‡], respectively; Tables S1-2 summarize their structural properties and CWA adsorption capacities. It is important to mention that accessibility of the pore space, thermal and chemical stability as well as hydrophobicity have been experimentally tested for most of the selected MOFs with very good results,[24,40] supporting our choice among the huge number of MOFs available in the database.
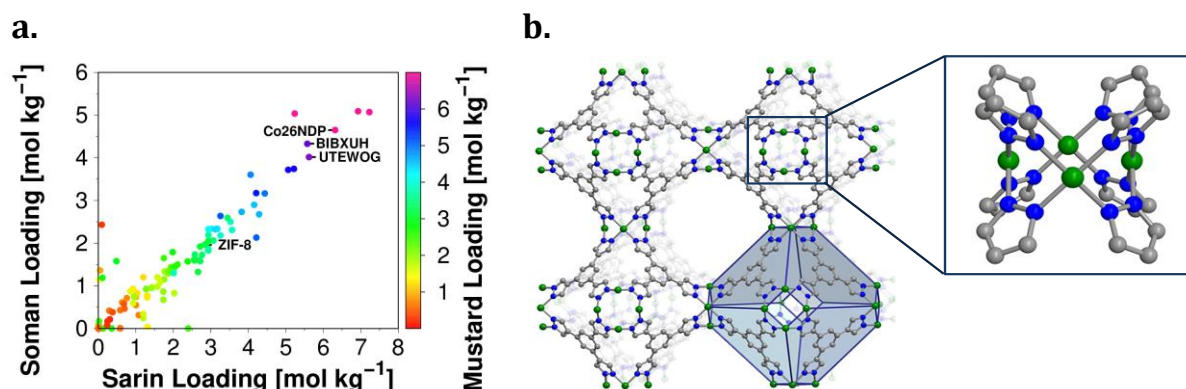
Figure 6. a. Comparison of the calculated mustard, sarin, and soman adsorption loading at 13.8 Pa (mustard) and 0.6 Pa (sarin and soman) in 156 hydrophobic MOFs at 298 K. **b.** Crystal structure of $[Ni_2(BTP)_3]$ (CSD code: UTEWOG). The inset shows the tetranuclear cluster of Ni(II) atoms and exo-bidentate pyrazolate linkers. Carbon, gray; nitrogen, blue; nickel, green. Hydrogen atoms have been omitted for simplification.

In order to confirm the applicability of our computational screening approach, and from the practical point of view, we selected $[Ni_3(BTP)_2]$ (CSD code: UTEWOG) for synthesis since it is regarded as one of the most thermally and chemically stable MOF materials.[40] The presence of low spin Ni(II) square planar metal centers in this system is a favourable feature in order to avoid water coordination to the activated material.[44] Next, we measured the breakthrough curve for DES adsorption of $[Ni_3(BTP)_2]$ at room temperature and 80% RH (Scheme S1) using a 20 mL min^{-1} flow of N_2 at RH 80% and 298 K containing 1 ppm of diethylsulphide (DES). Figure 7 shows that the DES reaches the saturation uptake in nearly 8 h, which is translated to an approximate uptake of 0.6 mol kg^{-1}. Moreover, the gas chromatography analysis indicates a significant drop of DES concentration in the eluted gas flow down to ca. 0.05 ppm. Consequently, it can be concluded that the DES relative pressure in equilibrium with the MOF material will be ca. 0.05 Pa with the adsorbed amount of DES agreeing reasonably well with the computational calculated values at the same range of pressure (0.617-1.193 mol kg^{-1} at pressure between 0.01 and 0.1 Pa).
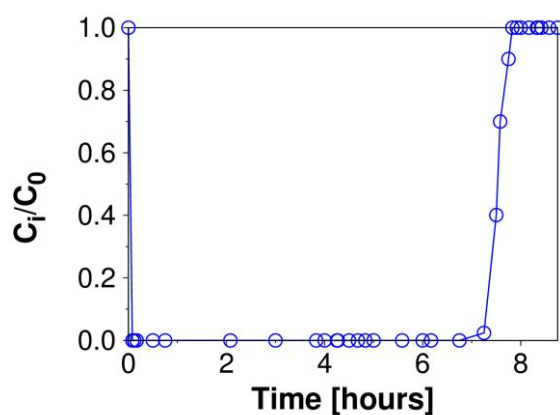

Figure 7. Breakthrough curve of 20 mL min^{-1} flow of N_2 at RH 80% and 298 K containing 1 ppm of diethylsulphide (DES) passed through chromatographic column packed with 150 mg of $[Ni_3(BTP)_2]$ (CSD code: UTEWOG).

8

We finally tested the capacity of the MOF to retain its original adsorption performance. For this, we evaluated the reversibility of the DES adsorption process by means of thermogravimetric analysis (TGA), diffuse reflectance and temperature programed desorption (Figures S10 and S11). The results indicate that DES is co-adsorbed with moisture giving rise to a $[Ni_3(BTP)_2]\cdot 4H_2O\cdot 0.5DES$ formulation as confirmed by TGA and temperature programed desorption. The higher affinity of the framework towards DES over moisture is confirmed by low temperature of the dehydration process (< 373 K), while DES desorption takes place at ca. 473 K. It should also be noted that neither the adsorbed water molecules nor the DES molecules gives rise to any modification of the metal coordination geometry as concluded from diffuse reflectance spectrum (Figure S12); showing an absorption at 450 nm characteristic of d-d transitions of low spin square planar Ni(II) pyrazolate systems.[45] This further suggests that physisorption in the MOF is solely responsible for the selective capture of DES over moisture.

3. Conclusions

In this work, we performed a high-throughput molecular simulation screening to explore the suitability of MOF structures for chemical warfare agent (CWA) protection: mustard, sarin, soman, and their commonly used simulants, and to identify an optimal material for further experimental test. We first selected 1,647 out of 2,932 MOFs structures provided in the DDEC database, with cavity diameter values larger enough to ensure accessibility of CWAs to the porous network. We then used the Widom insertion technique to evaluate efficiently the strength of the CWA-MOF interactions as a function of structural features such as pore size and surface area. We were able to demonstrate the good agreement between structure-property relationships for CWAs and their respective simulants, providing further support for the simulants use in experimental settings where the application of real CWAs is not possible. In particular, high CWA-MOF interactions were found in MOFs with reasonable high surface area (up to 2,000 $m^2\cdot g^{-1}$), whereas the highest K_H values were localized at between 5-6 Å. To minimize competitive water adsorption, we found 156 hydrophobic MOFs (ca. 10% of the studied MOFs) based on their water affinity using Widom insertion. We then run GCMC simulations were run for mustard, sarin, soman, and water at different pressures; we found negligible water loadings in the 156 hydrophobic MOFs at 80% of HR, supporting our fast screening approach based on Widom insertion. Out of 156 hydrophobic MOFs, we identified three optimal materials with adsorption capacities of > 4 $mol\cdot kg^{-1}$ for sarin, soman and mustard gas. All these materials showed larger surface areas (above 2,000 $m^2\cdot g^{-1}$) and LCDs (generally > 12 Å) than highlighted with Widom technique, what make sense since adsorption at the pressures under study is away from Henry´s region and larger pores allow maximizing loading capacities. Selected materials also present low water affinity and high stability through metal-pyzarolate coordinative bonds. Remarkably, this high-throughput computational selection is experimentally supported by experimental reports. We completed our hierarchical high-throughput materials discovery approach by successfully synthesizing and testing one of the top 4 structures identified from simulations: $[Ni_3(BTP)_2]$, CSD code: UTEWOG; breakthrough experiments confirmed selective adsorption of DES from the humid stream. Indeed, the exceptional adsorption selectivity and stability in the presence of humidity provided by experimental results on $[Ni_3(BTP)_2]$ is evident by the low temperature of the dehydration process and the absence of modifications on the metal coordination geometry showed in the diffuse reflectance spectrum. A schematic representation summarizing the full screening process is included in Figure 8. All in all, inspired by high-throughput computer simulations, our screening approach provides not only synthetic guidelines to make suitable materials for CWA capture but also demonstrates a rare case of materials discovery where a priori knowledge of predicted adsorption capacity leads to oriented designed and efficient identification of new adsorbent materials.
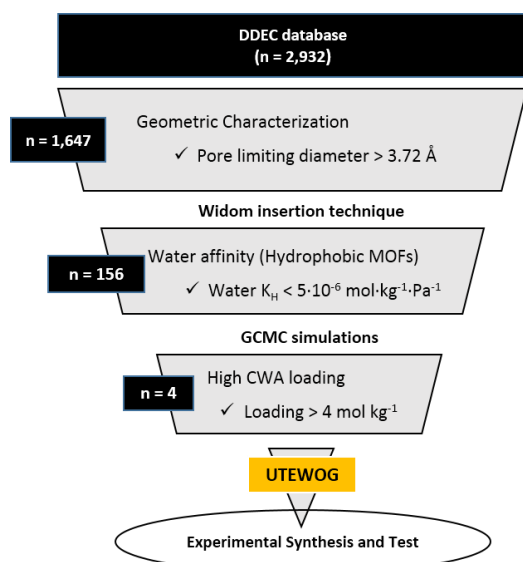
Figure 8. Schematic representation of the screening strategy followed in this work.

4. Methodology

The geometrical properties for all the MOFs were taken from the 2,932 experimentally synthesized MOF structures reported by Chung *et al.*[43]. The geometric characterization of each MOF structure was carried out for the largest cavity diameter (LCD), accessible pore volume (PV), and gravimetric surface area (GSA) using Zeo^{++}.[46] The reported GSAs were obtained using a probe of 3.72 Å diameter (corresponding to that of N$_2$),[31] and only included 1,647 out of 2,932 MOFs – those with pore regions accessible through windows large enough to admit N$_2$. This excludes MOFs where the chemicals under study do not access their pores.

All Monte Carlo simulations were performed using the code RASPA.[47] We first carried out Monte Carlo simulations in the canonical ensemble (CMC) using Widom test particle method[29] to evaluate helium void fraction as well as adsorbate-adsorbent interactions through Henry's constants (K_H) and isosteric heats of adsorption (Q_{st}). These simulations were carried out in the limit of zero loading with only one CWA molecule in the system. We used 40,000 production cycles for Widom insertion. Throughout this work, Q_{st} refers to the negative value of the enthalpy of adsorption, and therefore positive values are shown. GCMC simulations were performed to estimate adsorption loadings at room temperature. During each GCMC cycle, translation, rotation, insertions, deletions, and regrow moves are attempted, using 200,000 equilibration cycles and 200,0000 production cycles. The number of Monte Carlo steps per cycle equals the total number of molecules in the system with a minimum of 20 steps. Van der Waals interactions were described by 12-6 Lennard-Jones potential using a cutoff distance of 14 Å, where the interactions were truncated and analytical tail corrections were implemented. The force field parameters for water were taken from the TIP4P model;[48] TraPPE force field was used for DMMP, sarin, soman,[49] and DES.[50] The parameters for mustard gas were taken from Müller *et al.*[51] and those for DIFP from Vishnyakov *et al.*[52] Force field parameters for CWA and simulants are summarized in tables S3-S7. The Lennard-Jones parameters for the framework atoms were adopted from the Dreiding force field (DFF)[53] with the exception of metallic atoms, that were taken from the Universal Force Field (UFF).[54] All MOFs were treated as rigid in the simulations. Adsorbate-adsorbate and adsorbate-adsorbent van der Waals interactions were taken into account by Lorentz–Berthelot mixing rules.[55] Framework atomic charges were calculated by Nazarian *et al.* using plane-wave DFT calculations and

DDEC charge partitioning method.[30] Electrostatic interactions were considered by using Coulombic potentials and Ewald summations.

[Ni$_3$(BTP)$_2$] (UTEWOG) was synthetized according to Colombo *et al.*[40] Thermogravimetric, diffuse reflectance and XRPD analyses were used to determine the identity and phase purity of the material. TGA was carried out under air, on a Shimadzu-TGA-50H/DSC equipment, at a heating rate of 293 K min^{-1}. XRPD data were collected on a Bruker D2-PHASER diffractometer using CuKα radiation (λ = 1.5418 Å). The compounds were manually grounded in an agate mortar, then deposited in the hollow of a zero background silicon sample holder and measured.

For the evaluation of the dynamic adsorption of DES vapor at RH 80% by [Ni$_3$(BTP)$_2$] (Scheme S1). The [Ni$_3$(BTP)$_2$]·7.5H$_2$O material (166 mg) in microcrystalline form was packed in a stainless steel column, 5 cm length and 5 mm inner diameter. Afterward the material was activated at 523 K for 12 h under a 20 mlmin^{-1} He flow. Afterwards a constant flow of N$_2$ (4 mL min^{-1}) was bubbled in a flask containing DES at 303 K and then mixed with a N$_2$ flow (16 mL min^{-1}) bubbled in a flask containing distilled water at 303 K. Once, the composition of the gas mixture was stable it was flowed through the chromatographic column at room temperature. The DES content of the eluted gas flow was determined employing a flame ionization detector (FID) of a Varian 450-GC gas chromatograph.

The reversibility of the DES adsorption process was evaluated through TGA, XRPD, reflectance diffuse and temperature programed desorption using a heating ramp of 10 K min^{-1} and an Omnistar mass spectrometer.

Conflicts of interest

D.F.-J. has a financial interest in the start-up company Immaterial Labs, which is seeking to commercialize metal–organic frameworks.

Acknowledgements

Notes and References

‡Co26NDP corresponds to core-mof-ddec-365 from the work from Nazarian et al.; no CSD code was provided in the paper, and is not found in the CSD, which strongly suggests it is a hypothetical structure

1   L. F. Haber, *The Poisonous Cloud: Chemical Warfare in the First World War*, Oxford University Press, London, 1986.
2   J. B. Decoste and G. W. Peterson, *Chem. Rev.*, 2014, **114**, 5695–5727.
3   C. Montoro, F. Linares, E. Quartapelle Procopio, I. Senkovska, S. Kaskel, S. Galli, N. Masciocchi, E. Barea and J. A. R. Navarro, *J. Am. Chem. Soc.*, 2011, **133**, 11888–11891.
4   M. Enserink, *Science* , 2013, **341**, 1050–1051.
5   B. M. Smith, *Chem. Soc. Rev.*, 2008, **37**, 470–478.
6   Y. C. Yang, J. A. Baker and J. R. Ward, *Chem. Rev.*, 1992, **92**, 1729–1743.

7   A. M. Plonka, Q. Wang, W. O. Gordon, A. Balboa, D. Troya, W. Guo, C. H. Sharp, S. D. Senanayake, J. R. Morris, C. L. Hill and A. I. Frenkel, *J. Am. Chem. Soc.*, 2017, **139**, 599–602.

8   T. Grant Glover, G. W. Peterson, B. J. Schindler, D. Britt and O. Yaghi, *Chem. Eng. Sci.*, 2011, **66**, 163–170.

9   D. Britt, D. Tranchemontagne and O. M. Yaghi, *Proc. Natl. Acad. Sci. U. S. A.*, 2008, **105**, 11623–11627.

10   K. C. Kim, P. Z. Moghadam, D. Fairen-Jimenez and R. Q. Snurr, *Ind. Eng. Chem. Res.*, 2015, **54**, 3257–3267.

11   P. Ghosh, K. C. Kim and R. Q. Snurr, *J. Phys. Chem. C*, 2014, **118**, 1102–1110.

12   P. Z. Moghadam, D. Fairen-Jimenez and R. Q. Snurr, *J. Mater. Chem. A*, 2015, **4**, 529–536.

13   S. Galli, N. Masciocchi, V. Colombo, A. Maspero, G. Palmisano, F. J. López-Garzón, M. Domingo-Garcia, I. Fernández-Morales, E. Barea and J. A. R. Navarro, *Chem. Mater.*, 2010, **22**, 1664–1672.

14   N. S. Bobbitt, M. L. Mendonca, A. J. Howarth, T. Islamoglu, J. T. Hupp, O. K. Farha and R. Q. Snurr, *Chem. Soc. Rev.*, 2017.

15   H. C. Zhou, J. R. Long and O. M. Yaghi, *Chem. Rev.*, 2012, **112**, 673–674.

16   S. Kitagawa, R. Kitaura and S. Noro, *Angew. Chemie - Int. Ed.*, 2004, **43**, 2334–2375.

17   M. Eddaoudi, J. Kim, N. Rosi and O. M. Yaghi, *Science* , 2002, **295**, 469–472.

18   H. Furukawa, K. E. Cordova, M. O'Keeffe and O. M. Yaghi, *Science* , 2013, **341**, 974.

19   K. K. Tanabe and S. M. Cohen, *Chem. Soc. Rev.*, 2011, **40**, 498–519.

20   P. Z. Moghadam, A. Li, S. B. Wiggin, A. Tao, A. G. P. Maloney, P. A. Wood, S. C. Ward and D. Fairen-Jimenez, *Chem. Mater.*, 2017, **29**, 2618–2625.

21   J.-R. Li, R. J. Kuppler and H.-C. Zhou, *Chem. Soc. Rev.*, 2009, **38**, 1477–1504.

22   D. Britt, H. Furukawa, B. Wang, T. G. Glover and O. M. Yaghi, *Proc. Natl. Acad. Sci. U. S. A.*, 2009, **106**, 20637–20640.

23   R. Zou, R. Zhong, S. Han, H. Xu, A. K. Burrell, N. Henson, J. L. Cape, D. D. Hickmott, T. V Timofeeva, T. E. Larson and Y. Zhao, *J. Am. Chem. Soc.*, 2010, **132**, 17996–17999.

24   N. M. Padial, E. Quartapelle Procopio, C. Montoro, E. López, J. E. Oltra, V. Colombo, A. Maspero, N. Masciocchi, S. Galli, I. Senkovska, S. Kaskel, E. Barea and J. A. R. Navarro, *Angew. Chemie - Int. Ed.*, 2013, **52**, 8290–8294.

25   J. E. Mondloch, M. J. Katz, W. C. Isley III, P. Ghosh, P. Liao, W. Bury, G. W. Wagner, M. G. Hall, J. B. DeCoste, G. W. Peterson, R. Q. Snurr, C. J. Cramer, J. T. Hupp and O. K. Farha, *Nat Mater*, 2015, **14**, 512–516.

26   S. Y. Moon, E. Proussaloglou, G. W. Peterson, J. B. DeCoste, M. G. Hall, A. J. Howarth, J. T. Hupp and O. K. Farha, *Chem. - A Eur. J.*, 2016, **22**, 14864–14868.

27   P. Z. Moghadam, J. F. Ivy, R. K. K. Arvapally, A. M. dos Santos, J. C. Pearson, L. Zhang, E. Tyllianakis, P. Ghosh, I. W. H. Oswald, U. Kaipa, X. Wang, A. Wilson, R. Q. Snurr and M. Omary, *Chem. Sci.*, 2017, **0**, 1–12.

28   Y. J. Colon and R. Q. Snurr, *Chem. Soc. Rev.*, 2014, **43**, 5735–5749.

29   B. Widom, *J. Chem. Phys.*, 1963, **39**, 2808.

30   D. Nazarian, J. S. Camp and D. S. Sholl, *Chem. Mater.*, 2016, **28**, 785–793.

31   Y. S. Bae, A. O. Yazaydin and R. Q. Snurr, *Langmuir*, 2010, **26**, 5475–5483.

32   P. M. Schoenecker, C. G. Carson, H. Jasuja, C. J. J. Flemming and K. S. Walton, *Ind. Eng. Chem. Res.*, 2012, **51**, 6513–6519.

33   J. Cousinsaintremi, T. Rémy, V. Vanhunskerken, S. Vandeperre, T. Duerinck, M. Maes, D. Devos, E. Gobechiya, C. E. A. E. A. Kirschhock, G. V. V. Baron and J. F. M. F. M. Denayer, *ChemSusChem*, 2011, **4**, 1074–1077.

34   M. Spiandore, A. Piram, A. Lacoste, D. Josse and P. Doumenq, *Drug Test. Anal.*, 2014, **6**, 67–73.

35   S. Mérat, J. P. Perez, M. Rüttimann, E. Bordier, A. Lienhard, B. Lenoir and B. Pats, *Ann. Fr. Anesth. Reanim.*, 2003, **22**, 108–118.

36   Y. Seto, M. Kanamori-Kataoka, K. Tsuge, I. Ohsawa, K. Matsushita, H. Sekiguchi, T. Itoi, K. Iura, Y. Sano and S. Yamashiro, *Sensors Actuators, B Chem.*, 2005, **108**, 193–197.

37   A. Saxena, N. B. Hastings, W. Sun, P. A. Dabisch, S. W. Hulet, E. M. Jakubowski, R. J. Mioduszewski and B. P. Doctor, *Chem. Biol. Interact.*, 2015, **238**, 161–169.

38   S. O. Jacobsson, G. E. Cassel and S. a Persson, *Arch. Toxicol.*, 1999, **73**, 269–73.

39   H. J. Choi, M. Dincă and J. R. Long, *J. Am. Chem. Soc.*, 2008, **130**, 7848–7850.

40   V. Colombo, S. Galli, H. J. Choi, G. D. Han, A. Maspero, G. Palmisano, N. Masciocchi and J. R. Long, *Chem. Sci.*, 2011, **2**, 1311.

41   A. J. Howarth, Y. Liu, P. Li, Z. Li, T. C. Wang, J. T. Hupp and O. K. Farha, *Nat. Rev. Mater.*, 2016, **1**, 1–15.

42   J. A. Mason, J. Oktawiec, M. K. Taylor, M. R. Hudson, J. Rodriguez, J. E. Bachman, M. I. Gonzalez, A. Cervellino, A. Guagliardi, C. M. Brown, P. L. Llewellyn, N. Masciocchi and J. R. Long, *Nature*, 2015, **527**, 357–361.

43   Y. G. Chung, J. Camp, M. Haranczyk, B. J. Sikora, W. Bury, V. Krungleviciute, T. Yildirim, O. K. Farha, D. S. Sholl and R. Q. Snurr, *Chem. Mater.*, 2014, **26**, 6185–6192.

44   G. C. Shearer, V. Colombo, S. Chavan, E. Albanese, B. Civalleri, A. Maspero and S. Bordiga, *Dalt. Trans.*, 2013, **42**, 6450.

45   J. Klingele (née Hausmann), A. I. Prikhod'ko, G. Leibeling, S. Demeshko, S. Dechert and F. Meyer, *Dalt. Trans.*, 2007, 2003–2013.

46   T. F. Willems, C. H. Rycroft, M. Kazi, J. C. Meza and M. Haranczyk, *Microporous Mesoporous Mater.*, 2012, **149**, 134–141.

47   D. Dubbeldam, S. Calero, D. E. Ellis and R. Q. Snurr, *Mol. Simul.*, 2015, **42**, 81–101.

48   W. L. Jorgensen, J. Chandrasekhar, J. D. Madura, R. W. Impey and M. L. Klein, *J. Chem. Phys.*, 1983, **79**, 926.

49   N. Sokkalingam, G. Kamath, M. Coscione and J. J. Potoff, *J. Phys. Chem. B*, 2009, **113**, 10292–10297.

50   J. M. Stubbs, J. J. Potoff and J. I. Siepmann, *J. Phys. Chem. B*, 2004, **108**, 17596–17605.

51   T. J. Müller and F. Müller-Plathe, *J. Hazard. Mater.*, 2009, **168**, 13–24.

52   A. Vishnyakov, G. Y. Gor, M. T. Lee and A. V. Neimark, *J. Phys. Chem. A*, 2011, **115**, 5201–5209.

53   S. L. Mayo, B. D. Olafson and W. A. I. Goddard, *J. Phys. Chem.*, 1990, **101**, 8897–8909.

54   a. K. Rappe, C. J. Casewit, K. S. Colwell, W. a. Goddard and W. M. Skiff, *J. Am. Chem. Soc.*, 1992, **114**, 10024–10035.

55   M. P. Allen and D. J. Tildesley, *Computer Simulation of Liquids*, Oxford Clarendon Press, Oxford, 1987.